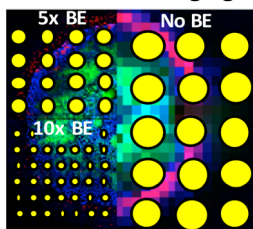


RESEARCH ARTICLE

Five Micron High Resolution MALDI Mass Spectrometry Imaging with Simple, Interchangeable, Multi-Resolution Optical System

Adam D. Feenstra,^{1,2} Maria Emilia Dueñas,^{1,2} Young Jin Lee^{1,2} ¹Department of Chemistry, Iowa State University, Ames, IA 50011, USA²Ames Laboratory-US DOE, Ames, IA 50011, USA5, 10, 50 μm Multi-Resolution Imaging

Abstract. High-spatial resolution mass spectrometry imaging (MSI) is crucial for the mapping of chemical distributions at the cellular and subcellular level. In this work, we improved our previous laser optical system for matrix-assisted laser desorption/ionization (MALDI)-MSI, from $\sim 9 \mu\text{m}$ practical laser spot size to a practical laser spot size of $\sim 4 \mu\text{m}$, thereby allowing for $5 \mu\text{m}$ resolution imaging without oversampling. This is accomplished through a combination of spatial filtering, beam expansion, and reduction of the final focal length. Most importantly, the new laser optics system allows for simple modification of the spot size solely through the interchanging of the beam expander component. Using 10 \times , 5 \times , and no beam expander, we could routinely change between ~ 4 , ~ 7 , and $\sim 45 \mu\text{m}$ laser spot size, in less than 5 min.

We applied this multi-resolution MALDI-MSI system to a single maize root tissue section with three different spatial resolutions of 5, 10, and $50 \mu\text{m}$ and compared the differences in imaging quality and signal sensitivity. We also demonstrated the difference in depth of focus between the optical systems with 10 \times and 5 \times beam expanders.

Keywords: Mass spectrometry imaging, MALDI, Laser spot size, Resolution, Maize, Root, Optics

Received: 19 September 2016/Revised: 17 November 2016/Accepted: 8 December 2016/Published Online: 3 January 2017

Introduction

Mass spectrometry imaging (MSI) has seen a surge in popularity as a biological imaging technique in the last decade because of its versatility, sensitivity, and label-free approach. These characteristics allow MSI to be applied to study a broad range of chemical compounds across a wide range of systems. This technique has been expanded to visualize compound classes such as lipids, proteins, and small molecules directly in plant and animal tissues [1–5]. General overviews of mass spectrometry imaging techniques can be found in various reviews [6–8].

Recently, high-resolution MSI has drawn enormous attention to visualize metabolites at a fine spatial resolution [9, 10]. The inherent characteristics of MS analysis combined with high-spatial resolution allow for detailed metabolite

information to be visualized in cellular and subcellular localization, offering unprecedented detail in terms of localization and metabolite composition of various tissue types. This type of information can be incredibly useful for complex tissue types such as plant tissue, where various metabolic processes utilizing hundreds of thousands of metabolites are highly sequestered among various cell types [11, 12].

In matrix-assisted laser desorption/ionization (MALDI)-MSI experiments, the achievable spatial resolution for a given analysis is largely determined by the spot size of the laser beam at the sample surface. As such, significant work has been focused on methods to reduce the laser spot size in order to increase the achievable spatial resolution. Early efforts have been made using coaxial laser optics within the time of flight mass spectrometer, which achieved down to $\sim 1 \mu\text{m}$ laser spot size for small molecules [13] or $\sim 7 \mu\text{m}$ size for proteins [14]. These approaches, however, could not maintain high sensitivity in limited sampling size, restricting their biological applications; hence, later works have been mostly focused on laser optics, without modifying mass analyzer. Spengler's group combined the coaxial laser optics with atmospheric pressure MALDI [15] and successfully applied it for 3–10 μm high-

Electronic supplementary material The online version of this article (doi:10.1007/s13361-016-1577-8) contains supplementary material, which is available to authorized users.

Correspondence to: Young J. Lee; e-mail: yjlee@iastate.edu

spatial resolution imaging [9, 16]. Another approach that achieves extremely high-spatial resolution is to utilize transmission geometry [17, 18]. In this instrumental setup, the laser beam is focused onto a sample tissue through the backside of microscope slides. This transmission geometry setup has been shown to focus the laser beam to less than 1 μm and MSI data acquisition was made down to 2.5 μm resolution [19].

Caprioli [20] and our own group [21] have previously reported a simple approach by modifying the laser optics of commercially available instruments to use a larger beam diameter and a shorter laser focal length. Both approaches utilized a spatial filter setup, where the laser beam is focused through a small diameter pinhole, to filter out non-Gaussian components of the beam. Combined, we were able to reduce the final laser spot size down to 5 μm , but the practical spot size was $\sim 9 \mu\text{m}$ to obtain sufficient ion signals, and we used oversampling (use of a raster step smaller than the laser spot size with complete depletion of analytes or matrix in each step [22]) to achieve 5 μm resolution MS imaging of maize leaf cross-sections. For these works, the laser burn mark was used as a measure of spatial resolution; however, there are some ambiguities in this approach. The line scan across a sharp edge has been used to better define the spatial resolution in secondary ion mass spectrometry [23]. This effort has been recently extended to MALDI-MS imaging with a specially designed pattern [24], but it is not available to most scientists yet. Hence, here we use the laser burn mark as a simple measure of the spatial resolution, even though it might measure slightly smaller than the actual resolution.

In this work, we improved our previous high-resolution optical setup to achieve a practical laser spot size below 5 μm , so that 5 μm high-resolution MALDI-MSI can be achieved without oversampling. Furthermore, the new setup allows easy change of the final spot size between ~ 4 , ~ 7 , and $\sim 45 \mu\text{m}$, through the simple interchange of the beam expander between 10 \times , 5 \times , and no beam expander, respectively. This multi-resolution setup is applied on maize root, and visualized various metabolites at spatial resolutions of 5, 10, and 50 μm , all on a single tissue section comparing analytical characteristics between the three resolution setups.

Experimental

Materials

2,5-Dihydroxybenzoic acid (DHB, 98%) was purchased from Sigma-Aldrich (St. Louis, MO, USA). Gelatin from porcine skin (300 bloom) was purchased from Electron Microscopy Sciences (Hatfield, PA, USA). A 1 mm diamond aperture (HP-3/8-DISC-DIM-1000) was purchased from Lenox Laser, Inc. (Glen Arm, MD, USA). A 60 mm focal length near UV achromatic lens (#65-977) and a 25/25.4 mm diameter lens mount (#56-354) were purchased from Edmund Optics (Barrington, NJ, USA). A 10 \times and 5 \times beam expander were purchased from ThorLabs Inc. (BE10x and BE5x; Newton, NJ,

USA). B73 inbred maize seeds were obtained courtesy of Dr. Marna Yandea-Nelson at Iowa State University.

Maize Root Growth and Sectioning

For MALDI-MSI analysis of root sections, inbred B73 maize seeds were grown using a procedure slightly modified from previously described methods [25]. Briefly, a row of seeds (embryo facing down) was arranged along the top edge of a moist paper towel. The paper towel was then rolled up and the bottom of the roll was placed into a 1 L beaker half filled with water. The seeds were allowed to grow for 10 d while kept in the dark. The beaker was checked periodically to ensure enough water remained to submerge the lower portion of the paper towel roll. After 10 d, the roots were collected and flash-frozen for the area of interest in liquid nitrogen to quench the metabolism. The frozen roots were then embedded in a 10% w/v gelatin solution in a cryo-mold and held in liquid nitrogen until the gelatin was mostly frozen. The roots were then moved to a cryostat (CM1520; Leica Biosystems, Buffalo Grove, IL, USA) with the temperature set at $-22 \text{ }^\circ\text{C}$, thermally equilibrated for 30 min, then cryo-sectioned at a thickness of 10 μm , and collected on adhesive tape windows (Leica).

Mass Spectrometry Imaging Analysis

A maize root section selected for MSI was initially placed onto a chilled aluminum block and lyophilized under moderate vacuum to prevent condensation as the section was brought to room temperature. A matrix layer of DHB was then deposited onto the gelatin sections by sublimation-vapor deposition, as has been previously described [26, at a temperature of 140 $^\circ\text{C}$ for 6 min.

The MALDI-MSI experiments were performed on a MALDI-linear ion trap (LIT)-Orbitrap mass spectrometer (MALDI-LTQ-Orbitrap Discovery; Thermo Finnigan, San Jose, CA, USA) modified to incorporate an external, 355 nm Nd:YAG laser (UVFQ; Elforlight, Daventry, UK). Three separate MS imaging runs were performed on the tissue section at different spatial resolutions of 5, 10, and 50 μm using a 10 \times , 5 \times , and no beam expander, respectively. The laser energy used was 84%, 87%, and 89%, respectively, optimized for each resolution setup with slightly higher laser energy required as the laser spot size increases. The same 10 laser shots were used per raster step for all three resolutions. Mass spectra were acquired in positive ion mode using an Orbitrap for a scan range of m/z 50–1000 at a mass resolution of 30,000 at m/z 400. After data acquisition, MS images were generated using ImageQuest software (Thermo Finnigan) and mass spectra were analyzed using Xcalibur (Thermo Finnigan). All images were generated using a mass tolerance of ± 0.005 and no normalization was applied.

MS/MS analysis was performed on an adjacent tissue section prepared identically to the one used for MS imaging. A multiplex imaging run [27] was performed at 50 μm resolution using no beam expander to collect MS/MS for multiple ions in a single run. The three ions shown in this work were analyzed

with a mass window of 1.0 Da. The collision energies were 125 for m/z 184.072, and 75 for m/z 365.102 and 426.077. All ions were activated for 30 ms.

Depth of Focus Experiment

A 10% w/v solution of gelatin was poured into a cryo-mold and frozen on liquid nitrogen. The gelatin was then cryo-sectioned at varying thicknesses and the sections were collected using adhesive tape windows. The sections were taped onto prechilled glass slides and stored at -80 °C. For spot size determination, the gelatin sections were prepared identically to those for imaging runs. Then, employing the various beam expander setups ($10\times$, $5\times$, and no beam expander), laser spots at varying energies were laid and measured through optical microscopy.

Safety Warning

Replacement of the manufacturer's enclosed laser system with an external laser such as the one described here results in a class IIIB laser system. Appropriate precautions should be taken when utilizing this system, including the use of appropriate eyewear and safety controls.

Results and Discussion

Modifications to Laser Optical System

In this work, the optics of a commercial MALDI-LIT-Orbitrap instrument were modified to achieve 5 μm high-resolution imaging, while also allowing for multi-resolution imaging through the interchanging of beam expanders. This work represents a significant improvement from our group's previous work, reducing the laser spot size for high-resolution MALDI-MSI applications. Descriptions of the original MALDI source [28] and our previous modification [21] can be found in earlier publications.

For a laser beam, the diffraction limited spot size is given by the following equation [20]:

$$D_s = M^2 \cdot \frac{4}{\pi} \cdot \lambda \cdot \frac{f}{D_b} \cdot \frac{1}{\cos\theta} \quad (1)$$

where D_s represents the diffraction limited spot size, M represents the beam quality factor ($M = 1$ for a perfect Gaussian beam), λ represents the laser wavelength, f represents the focal length of the focusing lens, D_b represents the input beam diameter to the final focusing lens, and $\cos\theta$ represents the incident angle of the laser beam on the sample.

Based on this equation, there are three main ways to reduce the laser spot size for a given optical system: (1) improving the beam quality factor (M closer to 1), (2) reducing the focal length of the focusing lens, and (3) increasing the input beam diameter. For the adjusted optical system in this work, all three factors were taken into consideration and optimized to the best of our abilities without requiring extensive instrumental

modifications. A schematic representation and photographs of the modified optical setup and source can be found in Figure 1a and b, respectively.

In our previous work [21], a home-built Keplerian configuration was employed as a beam expander. In this setup, the laser beam is focused down to a small spot, and then re-expanded to a bigger laser beam size. The laser beam in this home-built configuration was focused through a small diameter pinhole (25 μm) to remove significant non-Gaussian beam components. However, optical alignment to focus the laser beam through a 25 μm pinhole proved to be a very difficult and time-consuming process, and turned out to be problematic to interconvert between different laser spot sizes when more moderate resolution imaging was desired. Additionally,

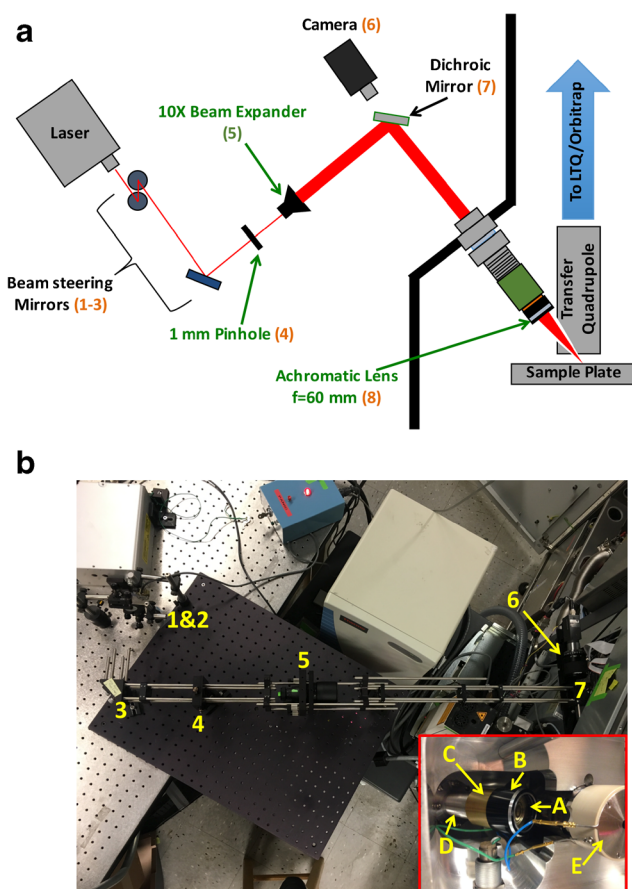


Figure 1. (a) Schematic of laser optic setup for high-resolution MS imaging. The laser is first passed through beam steering mirrors (1–3) before being filtered and expanded (4, 5). The laser is then passed into the instrument through the new focusing lens (7, 8). (b) Photograph of optical components with parts numbered as in 1a. The inset is a photograph of the source interior with modified optics. The focus lens (A) is placed into a compatible lens holder (B). The lens holder is threaded onto a custom-made male-female bronze intermediate (C), which is threaded onto a custom-made male rod attached to the flange (D). The beam passes through these optical components before passing through quadrupole and MALDI extraction plate (E), where it is then incident upon the MALDI sample plate (not shown)

focusing the laser beam down to a small enough spot size to fit through the pinhole increases the laser fluence and energy density, which we found can cause significant damage to a pinhole, even for those with a high-energy damage threshold.

In this work, to improve the beam quality factor (<1.2 initially, per manufacturer specifications), a 1 mm diameter pinhole (4) was placed into the beam path before the beam expander. Although this setup may not be as effective at removing non-Gaussian components compared with focusing through a small pinhole, it does remove the majority of the non-Gaussian laser beam components while avoiding the issues of aligning with a small opening as well as damage or destruction of the pinhole that arise from exposure to a highly focused laser beam.

The most important benefit of this setup is that we can adjust the laser spot size by simply changing the beam expander in a process that requires less than 5 min. For this work, we adopted commercially available Galilean configuration beam expanders with an encased, fixed geometry, which can be easily changed between different magnification beam expanders. To achieve the highest spatial resolution, a $10\times$ beam expander was inserted into the laser beam path (5), resulting in an expanded beam diameter of 10 mm, which is almost the maximum size that can pass through instrumental openings and into the final focus lens in the current geometry. The beam expander is positioned after the 1 mm pinhole and is held in place by a simple locking screw. As such, the beam expander can easily be inserted or removed as desired, allowing for a fast and simple way to change between input beam diameters and, therefore, final laser spot size.

Lastly, we modified the lens holder to position the focus lens as close as possible to the MALDI plate. The original focal length of the final lens was 125 mm [28], which we previously modified to accommodate a 100 mm focal length lens [21]. In this work, we further reduced the focal length down to 60 mm by integrating a custom-built lens holder into the source of the instrument. As the photograph in Figure 1b shows, the position of lens and lens holder can be adjusted by threading the bronze intermediate component in or out on the male rod; the optimum focal position for the smallest laser spot size was found by manually adjusting the z-position of the bronze intermediate (C). At the optimum position, the focus lens almost touches the outer case of the quadrupole ion lens.

All together, three optical modifications were made in this work, with the pinhole reducing the value of M close to 1, the beam expander increasing the value of D_b to 10 mm, and the final focus lens reducing the value of f to 60 mm. Assuming $M = 1.0$, Equation 1 gives the minimum achievable spot size as $3.2 \mu\text{m}$ with $f = 60 \text{ mm}$, $D_b = 10 \text{ mm}$, $\lambda = 0.355 \mu\text{m}$, and $\theta = 32^\circ$, dramatically improved from the original $\sim 50 \mu\text{m}$, and our previous work of $4.9 \mu\text{m}$. In our previous work, $\sim 5 \mu\text{m}$ laser spot sizes were obtained but without any ion signals (laser energy of 79%), and the practical laser spot size was $\sim 9 \mu\text{m}$ when the laser energy was increased to obtain sufficient ion signals for detection (laser energy of 80.5%). In the present work, a spot size as small as $\sim 3.4 \mu\text{m}$ was obtained with

sufficient ion signals (laser energy of 80%), while achieving the laser spot size close to the theoretical minimum (Figure 2). The laser spot size remained low, $\sim 4 \mu\text{m}$, even at the laser energy of 84% as shown later in the application to a maize root cross-section, suggesting we have an improvement of a factor of two in the laser spot size compared with our previous setup.

It needs to be mentioned that the MALDI sample plate is not completely level, and the position within the plate holder affects the laser spot size. Hence, we optimized laser focusing for the top portion of the left slide (our plate holder can load two microscope glass slides side by side) with an adhesive tape and a $10 \mu\text{m}$ thick tissue, and all the measurements were made at this position. The spot size is very reproducible at the same position even with multiple plate insertions and ejections. The laser spot size is significantly affected when another position is used for the $10\times$ beam expander, but the spot size change is minimal with $5\times$ beam expander with less than $10 \mu\text{m}$ spot sizes regardless of the position. The laser spot size is also greatly influenced by the tissue thickness for the $10\times$ beam expander (Supplementary Figure S1), to a much greater extent than we expected. This is partially attributed to the aberration halos, which are minimal when the laser is fully focused or a smaller beam size (e.g., $5\times$ beam expander) is used.

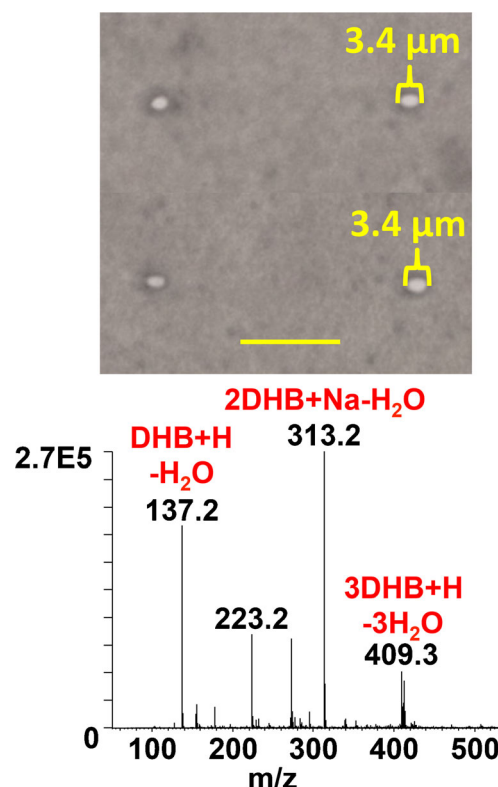


Figure 2. (Top) Microscope images of smallest laser spot size obtained on a thin layer of DHB. Laser spots here were generated using 10 laser shots at an energy of 80%. (Bottom) Ion trap mass spectrum obtained at the same time with the above laser spot size measurement, averaged from 47 spectra. Scale bar: $20 \mu\text{m}$

As will be further discussed in the next section, when a resolution of 5 μm is not necessary, a slightly more moderate resolution imaging run with 10 μm resolution using a 5 \times beam expander will be more convenient for routine imaging experiments. When the same experiment varying gelatin thickness was performed with the 5 \times beam expander (Supplementary Figure S1), the laser spot size was $\sim 7 \mu\text{m}$ with 10 μm thick gelatin and still only $\sim 8 \mu\text{m}$ with 5 or 15 μm thick gelatin. Even with the glass slide only without gelatin or adhesive tape, the laser spot size is increased only to $\sim 9 \mu\text{m}$. Compared with the experiments with the 10 \times beam expander, these spots laid on multiple sections were much more reproducible, confirming the larger depth of focus with a slightly lower resolution. These results indicate that, if necessary, we could vary the sample thickness on purpose to place the sample at the appropriate focal point when instrumental parameters are altered slightly, such as minute differences in mechanical z-position depending on the MALDI plate.

Multi-Resolution MS Imaging of a Maize Root Cross-Section

For the demonstration of high-resolution 5 μm MS imaging, the new laser optical system was applied to B73 maize roots grown

for 10 d. Plant roots are composed of a variety of tissue types (xylem, phloem, cortex, pith) on a small scale [29], of which the visualization of the fine structural features is attractive to demonstrate the current technological development. We have previously applied MS imaging for various plant tissue types, including flower [30], leaf [21, 31], seed [32], and root surface [30], but this is our first time analyzing root cross-sections.

Additionally, here we demonstrate an easy interchange between three different resolution setups and compare the differences in their analytical characteristics: 5 μm resolution using a 10 \times beam expander and $\sim 4 \mu\text{m}$ spot size, 10 μm resolution using a 5 \times beam expander and $\sim 7 \mu\text{m}$ spot size, and 50 μm resolution using no beam expander and $\sim 45 \mu\text{m}$ spot size. High-resolution imaging can provide detailed cellular and sub-cellular features of chemical distributions, but requires much longer data acquisition time and is expected to have limited sensitivity. In contrast, low resolution MS imaging can be done on a short time scale and with high sensitivity, but does not provide fine localization information. For this optical setup, the desired beam expander can be easily interchanged as the 10 \times beam expander is held in place by a single locking screw, while the 5 \times beam expander threads into a holder already incorporated into the optical system. As such, switching between the

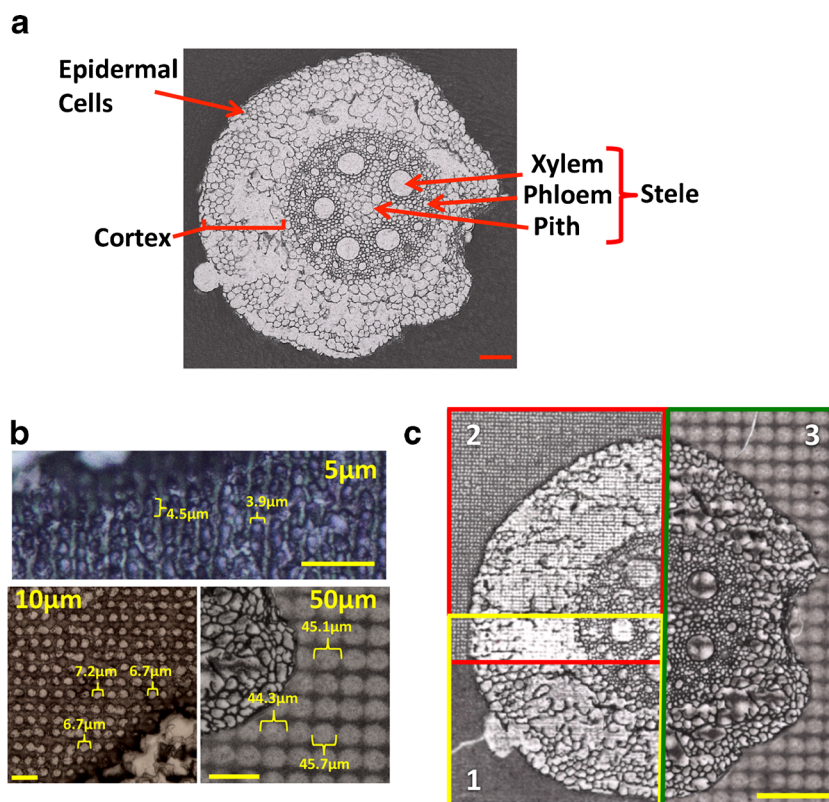


Figure 3. (a) Optical image of maize root cross-section with morphologic features labeled. Scale bar: 100 μm . (b) Ablation craters in gelatin areas for the 5, 10, and 50 μm imaging runs obtained from the imaging runs. Scale bar: 20 μm for the 5 and 10 μm runs; 100 μm for the 50 μm run. (c) Optical image of maize root cross-section after all three imaging runs. The 10 \times beam expander run (yellow) was performed first, followed by the 5 \times (red), and no beam expander (green) runs. The 5 \times run slightly overlapped the area covered by the 10 \times run to ensure complete tissue coverage, but the overlapping area for the 5 \times run is not used for MS image generation. Scale bar: 200 μm

three setups (10 \times , 5 \times , and no beam expander) was done in about 2–3 min in this experiment.

A single maize root cross-section was sublimated with DHB and analyzed in positive ion mode using three different resolution setups solely through the interchanging of the beam expander component of the optical system described in Figure 1. Using the 10 \times beam expander, a spot size of ~ 4 μm was achieved and an imaging run was performed with a raster step of 5 μm to ensure no oversampling occurred. Replacing the 10 \times beam expander with the 5 \times beam expander or using no beam expander generated laser spots on the order of ~ 7 or ~ 45 μm , respectively, and imaging runs were performed at raster step sizes of 10 and 50 μm . MS imaging took 4 h to image 1/4 of the root section in 5 μm resolution, 1.2 h to image another 1/4 of the root section in 10 μm resolution, and 0.2 h to image the remaining half of the root section in 50 μm resolution. Optical images of a maize root cross-section, ablation craters for imaging runs performed in this work, and an optical image of the root cross-section after the 3 imaging runs are shown in Figure 3.

MS images for three ions with distinct localization patterns from each of the imaging runs are presented together in Figure 4, with 50 μm images shown in the right half, 10 μm images in the top left quadrant, and the 5 μm images in the bottom left quadrant. The ions at m/z 184.072 and 365.102 are confidently identified as protonated phosphocholine and a sodiated disaccharide, respectively, through accurate mass

and MS/MS shown in Supplementary Figure S2. The identification of m/z 426.077 is tentatively assigned as potassiumated 2-hydroxy-4,7-dimethoxy-1,4-benzoxazin-3-one-glucoside (HDMBOA-Glc) based on accurate mass and MS/MS (Supplementary Figure S2), along with the presence of the corresponding deprotonated ion in negative mode with similar localization (not shown). This compound is known to present in maize [33] and previously seen in our MSI of maize leaf in negative mode [21].

In the 50 μm images of Figure 4 (the right half of root section), phosphocholine (m/z 184.072) appears to be localized throughout the entire root, whereas the disaccharide (m/z 365.102) appears to be evenly spread within the stele of the root. As the resolution is increased to the 10 and 5 μm images (the left half of root section), we are able to observe fine localization information that the disaccharide is localized mostly to the stele but also partially extended to the cortex, whereas the phosphocholine is localized throughout the root, but not homogeneously as it appears in 50 μm images. Meanwhile, the HDMBOA-Glc (m/z 426.077) appears to be distributed around the outer edges and epidermal cell layer of the root in the 10 and 50 μm images, but is barely seen in the 10 \times image as will be further discussed later.

A combination image is generated for these ions to further elucidate the fine spatial localization of the three metabolites. Looking at the 50 μm resolution combination image, the disaccharide (green) and phosphocholine (blue) appear to be

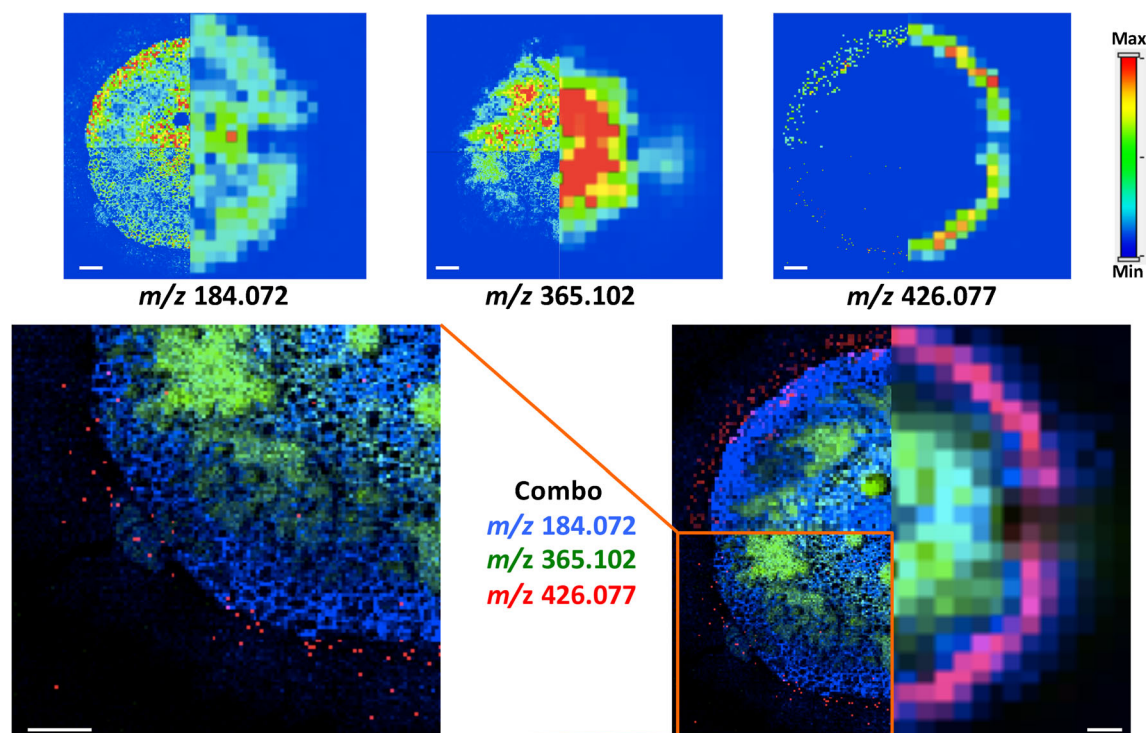


Figure 4. (Top) MS images for three selected ions of interest combined from each of the 5, 10, and 50 μm resolution imaging runs. (Bottom) Combination images of three MS images with different false colors. The 5 μm resolution image is enlarged to show the fine localization information. The max values used in generating the 5 and 10 μm resolution images are 1×10^6 , 5×10^5 , and 6×10^4 for m/z 184.072, 365.102, and 426.077, respectively, whereas 10 times higher max values are used for 50 μm resolution images. The scale bar is 100 μm

distributed between the inner stele and cortex of the root with some overlap (cyan color), whereas phosphocholine and HDMBOA-Glc (red) appear to be overlapping in the outer layers of the root (purple). In the 10 μm resolution image (top-left quadrant of the whole root section), we are able to determine that the disaccharide is localized within the xylem of the root in the inner stele and large porous region in the cortex, whereas phosphocholine is occupying the rest of the space in cortex and stele. Additionally, the image allows us to observe that phosphocholine and HDMBOA-Glc are co-localized in some part of the cortex layers (purple).

Lastly, in the 5 μm resolution image zoomed in and enlarged for better visualization, we can confirm the disaccharide is localized within the xylem tissues and surrounded by phosphocholine, but also find that neither the phosphocholine nor the disaccharide is localized within the small phloem tissues. This was not discernable at 10 μm resolution, and demonstrates the necessity of high-resolution capabilities for the elucidation of fine localization information. Individual cell walls can also be clearly observed within the stele and cortex layers using 5 μm resolution, as they are outlined by phosphocholine. In the case of HDMBOA-Glc, however, both the 50 and 10 μm resolution images show sufficient ion signal

to provide localization for this metabolite, whereas the 5 μm image shows little to no signal and is unable to provide clear localization.

For a better comparison of the spectral quality among the three different datasets, average mass spectra from each 1/4 of the root section were compared as shown in Figure 5a (for the no beam expander run, only half of the imaged root section was averaged to compare almost identical tissue areas). Foremost, it is apparent that the 50 μm resolution spectrum has significantly higher ion signals than either the 5 or 10 μm resolution spectra (8.7 or 4.8 times in total ion count, respectively), with the 10 μm resolution spectrum having higher ion signals than the 5 μm (~1.8 times in total ion count). This observation is not surprising considering a larger spot size results in a larger sampling area and, consequently, more ions shuttled into the mass spectrometer for analysis. It should be noted that the ion signals in the averaged spectra are not summed ion intensities but scaled by the number of spectra.

More precisely, the relation between sampling size and ion signal is more complicated than the simple description above, as it is also affected by laser fluence [34, 35]. As the laser spot size is reduced, higher laser fluence is needed to obtain sufficient ion signals, and ion signal increases as a power function

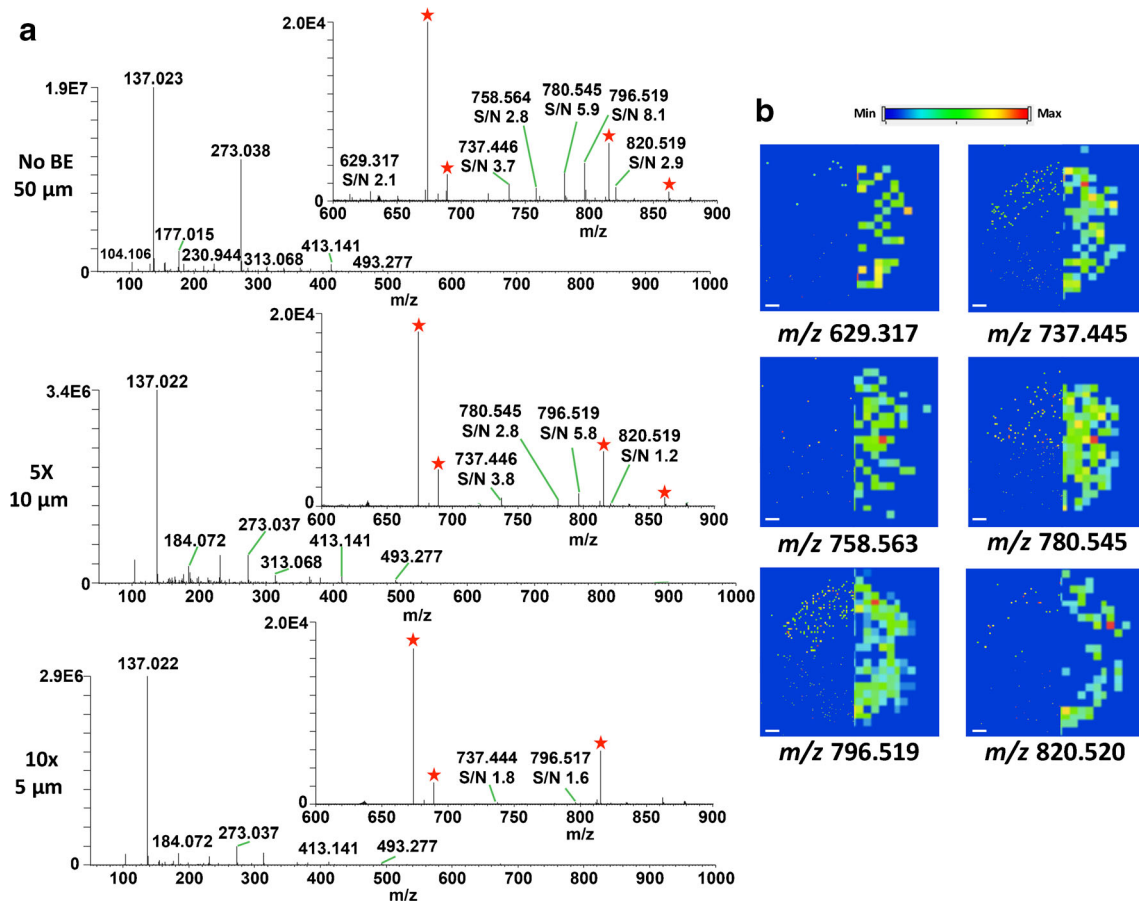


Figure 5. (a) The mass spectra obtained by 50 μm (top), 10 μm (middle), and 5 μm (bottom) resolution setup averaged over the 1/4 of root region. The mass range for m/z 600–900 is expanded as shown as inset spectra. Red stars denote background peaks. All real peaks with S/N values higher than 1 are labeled in the inset spectra. (b) MS images for the six ions labeled in the inset spectra of 5a. The scale bar is 100 μm

of laser fluence for the same laser spot size [34]. Compared at the optimum laser fluence, the ion yield per unit area is inversely proportional to the laser spot size, increasing with smaller laser spot size [36]. This agrees with our result in that the signal increase at a lower resolution is linearly proportional to the laser spot size, not the area. The optimum laser fluences used in this study are higher than typically reported, $\sim 1300 \text{ J/m}^2$ for $50 \mu\text{m}$ MS image and $\sim 18,000$ and $\sim 27,000 \text{ J/m}^2$ for 10 and $5 \mu\text{m}$ MS images, respectively. However, such high laser fluences are often reported when a Gaussian shape laser beam is used [35].

More significant differences are found for low abundance ions such as those in the inset spectra of Figure 5. In this high mass range ($>600 \text{ Da}$), six real ion peaks are clearly observed in $50 \mu\text{m}$ resolution spectrum at m/z 629, 737, 758, 780, 796, and 820 (all phosphatidylcholines or their fragments, except m/z 629, which is unidentified) with S/N above 2. It should be noted that the noise count displayed in the Qualbrowser software is over-represented. Therefore, the S/N reported here is expected to be about five times higher than the typical definition of S/N. At a higher resolution, the number of real ion peaks above S/N of 2 is decreased to 3 and 0 for 10 and $5 \mu\text{m}$ resolution setup, respectively, clearly demonstrating the decrease of sensitivity at higher resolution. The images for the six ions display results consistent with this observation (Figure 5b). All ions show clear images in the $50 \mu\text{m}$ resolution, but the image quality is dramatically deteriorated at higher resolution, with only three ions showing reasonable images in $10 \mu\text{m}$ resolution and none of them showing clear images in $5 \mu\text{m}$ resolution. These results are in line with recently published work demonstrating the effect of beam size related to total ion count [37].

These results demonstrate the tradeoff that comes with utilizing a small laser spot size for high-resolution mass spectrometry imaging. Although the spatial details that are gleaned are significantly increased for the high-resolution imaging, as shown in Figure 4, the ability to detect low abundance ions is reduced as seen in Figure 5. Depending on the analytes of interest, time constraints, and the required spatial resolution, low to moderate resolution imaging runs may be better suited in many cases. High-resolution analysis then can be used for those analytes that are highly abundant to further explore their fine spatial visualization.

Conclusions

This work represents a substantial advancement from our previous effort to reduce the laser spot size and, thus, achieve high-spatial resolution for MALDI-MSI. We have achieved a minimum laser spot size of $\sim 3.4 \mu\text{m}$, which is almost the ultimate limit possible in the current instrument without modifying the mass spectrometry ion optics. We have found that this setup has a serious limitation coming from the shallow depth of focus; nevertheless, we could still routinely obtain $\sim 4 \mu\text{m}$ laser spot size. The most significant advantage of this system from a

practical viewpoint is the simplicity with which the spatial resolution can be modified. A simple interconversion between different resolution setups is possible within a few minutes using $10\times$ beam expander for the high-resolution $5 \mu\text{m}$ imaging, $5\times$ beam expander for the medium-resolution $10 \mu\text{m}$ imaging, and no beam expander for low-resolution $50 \mu\text{m}$ imaging. The combination of the three-resolution setup is successfully demonstrated on a single root section, comparing analytical characteristics in terms of image quality and sensitivity.

With this improvement, we can now routinely perform ultra-high resolution MALDI-MSI as well as high-throughput, high-sensitivity, low-resolution MSI, and medium-throughput, moderate-resolution MSI experiments. While previously demonstrated instrumental setups have shown smaller ultimately achievable spot sizes on the order of $1 \mu\text{m}$ [13, 19], actual applications have been mostly performed with 5 or $10 \mu\text{m}$ spatial resolution due to the limited amounts of analytes available in a small sampling size. Plant samples are particularly challenging to obtain sufficient ion signals at high-resolution, and most applications are made at $5 \mu\text{m}$ or larger spatial resolution [16]. Considering this limitation, we believe our system is comparable to other top level systems in most high-resolution imaging applications. Furthermore, the ease of changing the spatial resolution is a strength of our system that most other optics systems do not offer. We expect we should be able to run various interesting applications in the future with this tunable capability of MALDI-MSI.

Acknowledgements

This work was supported by the US Department of Energy (DOE), Office of Basic Energy Sciences, Division of Chemical Sciences, Geosciences, and Biosciences. A special thanks to Terry Herrman and Alon Klekner of the Ames Laboratory for their assistance in designing and engineering the lens holder optical components. The Ames Laboratory is operated by Iowa State University under DOE contract DE-AC02-07CH11358.

References

1. Murphy, R.C., Hankin, J.A., Barkley, R.M.: Imaging of lipid species by MALDI mass spectrometry. *J. Lipid Res.* **50**, S317–S322 (2009)
2. Stoeckli, M., Chaurand, P., Hallahan, D.E., Caprioli, R.M.: Imaging mass spectrometry: a new technology for the analysis of protein expression in mammalian tissues. *Nat. Med.* **7**, 493–496 (2001)
3. Cha, S., Zhang, H., Ilarslan, H.I., Wurtele, E.S., Brachova, L., Nikolau, B.J., Yeung, E.S.: Direct profiling and imaging of plant metabolites in intact tissues by using colloidal graphite-assisted laser desorption/ionization mass spectrometry. *Plant J.* **55**, 348–360 (2008)
4. Li, Y., Shrestha, B., Vertes, A.: Atmospheric pressure infrared MALDI imaging mass spectrometry for plant metabolomics. *Anal. Chem.* **80**, 407–420 (2008)
5. Sturtevant, D., Lee, Y.-J., Chapman, K.D.: Matrix assisted laser desorption/ionization-mass spectrometry imaging (MALDI-MSI) for direct visualization of plant metabolites in situ. *Curr. Opin. Biotechnol.* **37**, 53–60 (2016)
6. van Hove, E.R.A., Smith, D.F., Heeren, R.M.: A concise review of mass spectrometry imaging. *J. Chromatogr.* **1217**, 3946–3954 (2010)

7. Lee, Y.J., Perdian, D.C., Song, Z., Yeung, E.S., Nikolau, B.J.: Use of mass spectrometry for imaging metabolites in plants. *Plant J.* **70**, 81–95 (2012)
8. Weaver, E.M., Hummon, A.B.: Imaging mass spectrometry: from tissue sections to cell cultures. *Adv. Drug Deliv. Rev.* **65**, 1039–1055 (2013)
9. Römpf, A., Spengler, B.: Mass spectrometry imaging with high resolution in mass and space. *Histochem Cell Biol.* **139**, 759–783 (2013)
10. Römpf, A., Guenther, S., Schober, Y., Schulz, O., Takats, Z., Kummer, W., Spengler, B.: Histology by mass spectrometry: label-free tissue characterization obtained from high-accuracy bioanalytical imaging. *Angew. Chem. Int. Ed.* **49**, 3834–3838 (2010)
11. Sumner, L.W., Mendes, P., Dixon, R.A.: Plant metabolomics: large-scale phytochemistry in the functional genomics era. *Phytochemistry* **62**, 817–836 (2003)
12. Goodacre, R., Vaidyanathan, S., Dunn, W.B., Harrigan, G.G., Kell, D.B.: Metabolomics by numbers: acquiring and understanding global metabolite data. *Trends Biotechnol.* **22**, 245–252 (2004)
13. Spengler, B., Hubert, M.: Scanning microprobe matrix-assisted laser desorption/ionization (SMALDI) mass spectrometry: instrumentation for sub-micrometer resolved LDI and MALDI surface analysis. *J. Am. Soc. Mass Spectrom.* **13**, 735–748 (2002)
14. Chaurand, P., Schriver, K.E., Caprioli, R.M.: Instrument design and characterization for high resolution MALDI-MS imaging of tissue sections. *J. Mass Spectrom.* **42**, 476–489 (2007)
15. Koestler, M., Kirsch, D., Hester, A., Leisner, A., Guenther, S., Spengler, B.: A high-resolution scanning microprobe matrix-assisted laser desorption/ionization ion source for imaging analysis on an ion trap/Fourier transform ion cyclotron resonance mass spectrometer. *Rapid Commun. Mass Spectrom.* **22**, 3275–3285 (2008)
16. Bhandari, D.R., Wang, Q., Friedt, W., Spengler, B., Gottwald, S., Rompp, A.: High resolution mass spectrometry imaging of plant tissues: towards a plant metabolite atlas. *Analyst.* **140**, 7696–7709 (2015)
17. Zavalin, A., Todd, E.M., Rawhouser, P.D., Yang, J., Norris, J.L., Caprioli, R.M.: Direct imaging of single cells and tissue at sub-cellular spatial resolution using transmission geometry MALDI MS. *J. Mass Spectrom.* **47**, 1473–1481 (2012)
18. Thiery-Lavenant, G., Zavalin, A.I., Caprioli, R.M.: Targeted multiplex imaging mass spectrometry in transmission geometry for subcellular spatial resolution. *J. Am. Soc. Mass Spectrom.* **24**, 609–614 (2013)
19. Zavalin, A., Yang, J., Hayden, K., Vestal, M., Caprioli, R.M.: Tissue protein imaging at 1 μm laser spot diameter for high spatial resolution and high imaging speed using transmission geometry MALDI TOF MS. *Anal. Bioanal. Chem.* **407**, 2337–2342 (2015)
20. Zavalin, A., Yang, J.H., Caprioli, R.: Laser beam filtration for high spatial resolution MALDI imaging mass spectrometry. *J. Am. Soc. Mass Spectrom.* **24**, 1153–1156 (2013)
21. Korte, A.R., Yandean-Nelson, M.D., Nikolau, B.J., Lee, Y.J.: Subcellular-level resolution MALDI-MS imaging of maize leaf metabolites by MALDI-linear ion trap-Orbitrap mass spectrometer. *Anal. Bioanal. Chem.* **407**, 2301–2309 (2015)
22. Jurchen, J.C., Rubakhin, S.S., Sweedler, J.V.: MALDI-MS imaging of features smaller than the size of the laser beam. *J. Am. Soc. Mass Spectrom.* **16**, 1654–1659 (2005)
23. Senoner, M., Wirth, T., Unger, W., Osterle, W., Kaiander, I., Sellin, R.L., Bimberg, D.: BAM-L002—a new type of certified reference material for length calibration and testing of lateral resolution in the nanometre range. *Surf. Interface Anal.* **36**, 1423–U1429 (2004)
24. Zubair, F., Prentice, B.M., Norris, J.L., Laibinis, P.E., Caprioli, R.M.: Standard reticle slide to objectively evaluate spatial resolution and instrument performance in imaging mass spectrometry. *Anal. Chem.* **88**, 7302–7311 (2016)
25. Hetz, W., Hochholdinger, F., Schwall, M., Feix, G.: Isolation and characterization of *rtcs*, a maize mutant deficient in the formation of nodal roots. *Plant J.* **10**, 845–857 (1996)
26. Korte, A.R.Y., Gargey B.Feenstra, Adam D.Lee, Young Jin: Multiplex MALDI-MS imaging of plant metabolites using a hybrid MS system. In *Mass Spectrometry Imaging of Small Molecules*, He, L. Ed. Springer: New York, 2015; pp. 46–62.
27. Perdian, D.C., Lee, Y.J.: Imaging MS methodology for more chemical information in less data acquisition time utilizing a hybrid linear ion trap-Orbitrap mass spectrometer. *Anal. Chem.* **82**, 9393–9400 (2010)
28. Strupat, K., Kovtoun, V., Bui, H., Viner, R., Stafford, G., Horning, S.: MALDI produced ions inspected with a linear ion trap-Orbitrap hybrid mass analyzer. *J. Am. Soc. Mass Spectrom.* **20**, 1451–1463 (2009)
29. Hochholdinger, F., The Maize Root System: Morphology, Anatomy, and Genetics. In *Handbook of Maize: Its Biology*, Bennetzen, J. L.; Hake, S. C., Eds. Springer: New York, 2009; pp. 145–160.
30. Jun, J.H., Song, Z., Liu, Z., Nikolau, B.J., Yeung, E.S., Lee, Y.J.: High-spatial and high-mass resolution imaging of surface metabolites of *Arabidopsis thaliana* by laser desorption-ionization mass spectrometry using colloidal silver. *Anal. Chem.* **82**, 3255–3265 (2010)
31. Klein, A.T., Yagnik, G.B., Hohenstein, J.D., Ji, Z., Zi, J., Reichert, M.D., MacIntosh, G.C., Yang, B., Peters, R.J., Vela, J.: Investigation of the chemical interface in the soybean-aphid and rice-bacteria interactions using MALDI-mass spectrometry imaging. *Anal. Chem.* **87**, 5294–5301 (2015)
32. Feenstra, A.D., Hansen, R.L., Lee, Y.J.: Multi-matrix, dual polarity, tandem mass spectrometry imaging strategy applied to a germinated maize seed: toward mass spectrometry imaging of an untargeted metabolome. *Analyst* **140**, 7293–7304 (2015)
33. Niemeyer, H.M.: Hydroxamic acids (4-hydroxy-1, 4-benzoxazin-3-ones), defense chemicals in the *Gramineae*. *Phytochemistry* **27**, 3349–3358 (1988)
34. Dreisewerd, K., Schürenberg, M., Karas, M., Hillenkamp, F.: Influence of the laser intensity and spot size on the desorption of molecules and ions in matrix-assisted laser desorption/ionization with a uniform beam profile. *Int. J. Mass Spectrom. Ion Process* **141**, 127–148 (1995)
35. Guenther, S., Koestler, M., Schulz, O., Spengler, B.: Laser spot size and laser power dependence of ion formation in high resolution MALDI imaging. *Int. J. Mass Spectrom.* **294**, 7–15 (2010)
36. Qiao, H., Spicer, V., Ens, W.: The effect of laser profile, fluence, and spot size on sensitivity in orthogonal-injection matrix-assisted laser desorption/ionization time-of-flight mass spectrometry. *Rapid Commun. Mass Spectrom.* **22**, 2779–2790 (2008)
37. Wiegelmann, M., Dreisewerd, K., Soltwisch, J.: Influence of the laser spot size, focal beam profile, and tissue type on the lipid signals obtained by MALDI-MS imaging in oversampling mode. *J. Am. Soc. Mass Spectrom.* 1–13 (2016)